



This open access document is posted as a preprint in the Beilstein Archives at <https://doi.org/10.3762/bxiv.2024.19.v1> and is considered to be an early communication for feedback before peer review. Before citing this document, please check if a final, peer-reviewed version has been published.

This document is not formatted, has not undergone copyediting or typesetting, and may contain errors, unsubstantiated scientific claims or preliminary data.

Preprint Title Numerical study of magnetic properties for Co-Fe-Nb nanofilms as promising materials for magnetoresistive memory

Authors Alexander Vakhrushev, Aleksey Y. Fedotov, Olesya Severyukhina, Anastasia Salomatina, Vladimir Boian and Anatolie Sidorenko

Publication Date 28 März 2024

Article Type Full Research Paper

ORCID® iDs Aleksey Y. Fedotov - <https://orcid.org/0000-0002-0463-3089>; Olesya Severyukhina - <https://orcid.org/0000-0001-6014-9462>; Anastasia Salomatina - <https://orcid.org/0000-0003-4104-6454>; Vladimir Boian - <https://orcid.org/0000-0002-7653-5779>



License and Terms: This document is copyright 2024 the Author(s); licensee Beilstein-Institut.

This is an open access work under the terms of the Creative Commons Attribution License (<https://creativecommons.org/licenses/by/4.0>). Please note that the reuse, redistribution and reproduction in particular requires that the author(s) and source are credited and that individual graphics may be subject to special legal provisions.

The license is subject to the Beilstein Archives terms and conditions: <https://www.beilstein-archives.org/xiv/terms>.

The definitive version of this work can be found at <https://doi.org/10.3762/bxiv.2024.19.v1>

Numerical study of magnetic properties for Co-Fe-Nb nanofilms as promising materials for magnetoresistive memory

Alexander Vakhrushev¹, Aleksey Fedotov*^{1,2}, Olesya Severyukhina^{1,2}, Anastasia Salomatina^{1,2}, Vladimir Boian³, and Anatolie Sidorenko³

Address: ¹Institute of Mechanics, Udmurt Federal Research Center, Ural Division, Russian Academy of Sciences, Baramzinoy 34, Izhevsk 426067, Russia, ²Nanotechnology and Microsystems Department, Kalashnikov Izhevsk State Technical University, Studencheskaya 7, Izhevsk 426069, Russia, ³Technical University of Moldova, Institute of Electronic Engineering and Nanotechnologies, Academiei 3/3, Chisinau 2028 Moldova

Email:

Aleksey Fedotov* - alezfed@gmail.com

* Corresponding author

Abstract

The paper presents an overview of the magnetic resistive memory varieties, discusses their design features, weaknesses and benefits, and provides a comparative characteristic. A review of a combined mathematical model that jointly describes the change of spins and coordinates of atoms (spin-lattice dynamics) is given. In general, the model can use any form of interatomic force potential and

describes various contributions to the magnetic Hamiltonian. In this work, a simplified form of the magnetic Hamiltonian, taking into account only the Zeeman and exchange interactions, was considered to investigate magnetic interactions. The described model is implemented in the SPIN software package in the freely distributed LAMMPS complex. In this work, computational experiments were performed using the MEAM potential. The computational experiments represent three separate series of calculations. In the first one, the formation and structuring processes in a multilayer cobalt-iron-niobium nanocomposite were considered. It was shown that during the deposition of niobium, a rough nanofilm is formed, with height differences of several angstroms. It was noted that between the nanofilms of iron and niobium, the formation of a more diffuse contact zone was observed, compared to the contact of the layers of cobalt and iron. In the second version of the numerical experiments, the mutual self-ordering of directions and reorientation of spins in crystalline iron were analyzed, both in the presence of an external magnetic field and in its absence. During the simulation, the formation of vortex flows (skyrmions) was revealed. It was shown that under the influence of an external magnetic field an induced magnetic moment occurs in crystalline iron. Its direction is opposite to the direction of the magnetic induction vector of the applied field. The third numerical experiment was focused on modeling the magnetic properties of the cobalt-iron bilayer film under the conditions of a uniform external magnetic field. The formation of skyrmions was more typical for the Fe layer. Clearly defined magnetic domain regions were obtained in the cobalt nanofilm. It was revealed that the total magnetization of the Co-Fe system is low due to the absence of a clearly defined priority direction of the magnetic moments.

Keywords

Spintronics, mathematical modeling, molecular dynamics, MEAM, LAMMPS, spin dynamics, MRAM, ferromagnetics, spin valve, skyrmions

Introduction

The demands on modern semiconductor electronics and microelectronics are increasing every year. This is due to the fact that the amount of data to be processed and stored is constantly growing. Currently, artificial intelligence (AI) is actively being used in many areas of science and technology to find solutions to certain problems. For example, researchers in the field of genetics use neural networks to study patterns of heredity and changes in organisms of living beings [1]. Since AI processes huge amounts of data, it needs large memory and energy capacities, as well as improved performance of individual elements in computing systems. At the moment, computing devices are no longer successful enough to cope with the increasing heat dissipation of chips and high power consumption. In the near future it is not excluded that the world will face inefficiency of modern information processing and storage devices when solving tasks with large data sets. In connection with the above-mentioned there is an extreme necessity in development of new ways for processing and storage of information. And these methods should include both the search for new materials for devices and the approach to recording and reading information from a completely different side.

There are several directions of research on the issue at hand. Many scientists believe that quantum computers [2] will change the current state of affairs because they are much faster in solving special tasks than computers built on semiconductor electronics. However, the problem is that quantum computers are designed

specifically for certain tasks, such as factorizing numbers, and do not have much advantage in solving everyday tasks. Other researchers suggest that the way out is to improve existing devices rather than inventing new ones. An example of this can be considered quantum cellular automata [3], which can replace conventional transistors.

Also, one of the possible solutions to the problem is considered to be a departure from the von Neumann architecture, a principle in which programs and data are stored in the same memory. The main problem of this architecture is the limitation in the bandwidth of the data between the processor and the shared memory area, the so-called "bottle neck". This limitation significantly reduces the performance and power of the computing system. The problem within the existing architecture is usually solved by introducing a caching mechanism, but such modernization leads to higher cost of electronic devices and increases the risk of side errors. For this reason, one of the main and very promising directions in non-von Neumann architecture is spintronics. Spintronic devices are much more efficient than semiconductor electronics devices by using the spin of an electron rather than its charge to record information. They use much less energy, and the density of information recording is many times higher. Spintronics materials can be based on various mechanisms and phenomena, such as the effect of giant magnetoresistance [4] or tunneling magnetoresistance. Currently, these effects are already used in tunneling magnetoresistive sensors in hard disk read heads. This has been responsible for a significant increase in the information storage density of hard disks [5]. In addition, more and more efforts are being made to develop different types of magnetoresistive random access memory (MRAM) [6-8].

One of the main tasks for spintronics is the search for new promising materials. An alternative name for spintronics is magnetoelectronics, as a result materials for

spintronic devices should have a number of magnetic properties. Therefore, ferromagnetics in various heterostructured systems such as ferromagnetic-paramagnetic [9], ferromagnetic-superconductor [10], ferromagnetic-antiferromagnetic [11] are considered as one of the most common materials.

At the moment, there is an active search for combinations of elements and materials for spintronics heterostructures. Antiferromagnetics (AFM) in combination with ferromagnetics, for example, give good results for writing information, although they do not have high efficiency in reading, and the ferromagnetic-superconductor structure faces a number of limitations due to differences in operating temperatures and the Meissner effect.

The purpose of this work is to study the formation processes, structure and properties of nanomaterials for spintronics devices by using theoretical methods with the help of mathematical modeling. The work is a development of earlier studies of the formation processes for photovoltaic converters [12], multilayer superconductor-ferromagnetic nanostructures [13-15], the growth of ordered arrays of luminescent matrices based on templates made of porous aluminum oxide [16], the technology of creating composite nanoparticles for special purposes and probabilistic analysis of the mechanisms of their formation and growth [17].

Magnetoresistive memory has proven to be one of the most efficient, least power-consuming, and quite compact. The MRAM structure is based on a spin valve with giant magnetoresistance and consists of three layers: two ferromagnetic layers and an insulating nanofilm between them. The magnetization direction of one layer of the ferromagnetic is fixed, while the other layer is free and can change its magnetization direction. If the direction of magnetization of the films coincides, the resistance of the insulating layer becomes minimal and the electron easily passes through it. Otherwise, the resistance is maximum and the current flows with difficulty.

Table 1 summarizes the comparative characteristics of different varieties of magnetoresistive memory. Each of them has a number of advantages as well as a number of disadvantages, especially it concerns difficulties in the process of its production. At the moment only three types of magnetoresistive memory have been actually realized out of the presented ones - Toggle-MRAM, STT-MRAM and SOT-MRAM, the rest are under development. Due to its non-volatile nature and the ability to store data for a very long time, these types of MRAM can be used in personal computers, smartphones, aerospace and military systems, smart cards, as well as in special devices for data recording, the so-called flight recorders.

Table 1: Comparative characterization of MRAM

| Characteristics | Toggle-MRAM | SOT-MRAM | STT-MRAM | TA-MRAM | EB-MRAM |
|-----------------|--|---|--|--|---|
| Performance | ~35 nc [20] | 0,2 nc [21] | ~10 nc [22] | 0,5 nc [18] | ~10 nc [19] |
| Cell dimension | 130 nm | 60-80 nm | 45 nm | 65 nm | - |
| Advantages | <ul style="list-style-type: none"> - thermal stability; - durability; - wide temperature range; | <ul style="list-style-type: none"> - increased durability; - switching speed; - reliability; | <ul style="list-style-type: none"> - the change in magnetization is due to spin momentum transfer, not to an external magnetic field; | <ul style="list-style-type: none"> - thermostability; - recording selectivity; - immunity to external magnetic field; | <ul style="list-style-type: none"> - switching is carried out without an external magnetic field; - high threshold density; - potential application in neuromorphic computing; |
| Disadvantages | <ul style="list-style-type: none"> - an external magnetic field is required; | <ul style="list-style-type: none"> - difficulty in production; | <ul style="list-style-type: none"> - long incubation time; - low durability; - difficulty in production; | <ul style="list-style-type: none"> - energy consumption is not optimized; - the choice of materials is limited; | <ul style="list-style-type: none"> - production labor intensity |

In any of the presented varieties of memory it is possible to use the ferromagnetic-superconductor structure as a spin valve or magnetic tunnel junction. Using the apparatus of mathematical modeling can be found such a composition and structure

of memory cells, in which their disadvantages can be reduced or minimized, and the characteristics of memory devices can be optimized.

Spin dynamics model

Computational experiments remain an important tool for the prediction and theoretical understanding of various phenomena in magnetic materials. Molecular dynamics methods have been and still are intensively used to study phase diagrams, critical phenomena, structural properties and dynamic behavior of nanomaterials.

Consider a system consisting of N magnetic particles (atoms) of mass m_i , described by the generalized Hamiltonian in the form (1) [23-25]:

$$\hat{H} = \hat{H}_{\text{lat}} + \hat{H}_{\text{mag}}, \quad (1)$$

where \hat{H}_{lat} and \hat{H}_{mag} – Hamiltonians of the lattice subsystem, which takes into account the spatial motion of atoms, and the magnetic subsystem.

For the microcanonical ensemble (NVE), which is used for representing systems with fixed composition, volume and total energy, the Hamiltonian can be written as a following expression:

$$\hat{H} = \sum_{i=1}^N \frac{m_i \mathbf{v}_i^2}{2} + U(\mathbf{r}) - \sum_{i,j,i \neq j}^N J(r_{ij}) \mathbf{s}_i \cdot \mathbf{s}_j, \quad (2)$$

where \mathbf{r}_i and \mathbf{v}_i – radius-vector and velocity of the i -th atom, $U(\mathbf{r})$ – atomic interaction potential, $J(r_{ij}) > 0$ – exchange integral for a pair of spins located at a distance $r_{ij} = |\mathbf{r}_{ij}| = |\mathbf{r}_j - \mathbf{r}_i|$, \mathbf{s}_i – unit spin vector of each atom. The first two terms in (2) define the mechanical behavior of atoms, the last one describes the change of magnetic degrees of freedom.

In accordance with the approach proposed by V.P. Antropov and his co-authors [26, 27], the system is considered as a set of atoms, each of which is associated with

a spin vector \mathbf{s}_i . The connection of the ordinary spin vector with the normalized one is carried out by means of the relation:

$$\mathbf{S}_i = \hbar g_i \mathbf{s}_i, \quad (3)$$

where \hbar – reduced Planck constant, g_i – Lande multiplier of the i -th spin.

The relaxation processes in the magnetomechanical system were modeled using the Langevin equation [28, 29] and the stochastic Landau-Lifshitz-Hilbert equation [25, 30]. The joint solution of these equations is the basis of the spin dynamics model of particles used in this work:

$$m_i \frac{d\mathbf{v}_i}{dt} = \mathbf{\Phi}_i - \kappa \mathbf{v}_i + \boldsymbol{\chi}(t), \quad \mathbf{\Phi}_i = -\nabla U(\mathbf{r}) = -\frac{\partial U(\mathbf{r})}{\partial \mathbf{r}_i}, \quad (4)$$

$$\frac{d\mathbf{s}_i}{dt} = \frac{1}{(1+\lambda^2)} \left((\boldsymbol{\omega}_i + \boldsymbol{\eta}(t)) \times \mathbf{s}_i + \lambda \mathbf{s}_i \times (\boldsymbol{\omega}_i \times \mathbf{s}_i) \right), \quad i = 1, 2, \dots, N \quad (5)$$

where $\mathbf{\Phi}_i$ are interatomic forces caused by the action of the potential gradient $U(\mathbf{r})$, κ is coefficient of viscous friction force proportional to the atom velocity \mathbf{v}_i , $\boldsymbol{\chi}(t)$ is white noise, participating in the description of the stochastic process of atomic motion and arising due to collisions of particles, λ is damping spin coefficient, $\boldsymbol{\eta}(t)$ is white noise characterizing spin behavior of the system, $\boldsymbol{\omega}_i$ is the gyromagnetic ratio multiplied by the local magnetic field in which the spin is located. The latter value can be calculated in accordance with the expression [25]:

$$\boldsymbol{\omega}_i = -\frac{1}{\hbar} \frac{\partial \hat{H}_{\text{mag}}}{\partial \mathbf{s}_i}. \quad (6)$$

It was shown earlier by the authors [31-33] that thermal and magnetic fluctuations are well described in the context of the Langevin approach. In the context of this approach the random forces $\boldsymbol{\chi}(t)$ and $\boldsymbol{\eta}(t)$ are given with characteristic first and second moments:

$$\langle \chi(t) \rangle = 0, \quad \langle \chi_\alpha(t) \chi_\beta(t') \rangle = D_l \delta_{\alpha\beta} \delta(t-t'), \quad D_l = \frac{2k_B T_l}{B}, \quad (7)$$

$$\langle \eta(t) \rangle = 0, \quad \langle \eta_\alpha(t) \eta_\beta(t') \rangle = D_s \delta_{\alpha\beta} \delta(t-t'), \quad D_s = \frac{2\pi\lambda k_B T_s}{\hbar}, \quad (8)$$

where α and β are vector components, t and t' are different time periods, $\delta(t-t')$ is Dirac delta function, D_l and D_s are amplitudes of coordinate and spin random oscillations, k_B is Boltzmann constant, B is Brownian motion, T_l and T_s are ordinary (lattice) and spin temperatures.

A simple expression for the magnetic Hamiltonian of N interacting particles possessing spins is defined by the expression:

$$\hat{H}_{\text{mag}} = \hat{H}_Z + \hat{H}_{\text{ex}} = -\mu_B \mu_0 \sum_{i=1}^N g_i \mathbf{s}_i \cdot \mathbf{H}_{\text{ext}} - \sum_{i,j,i \neq j}^N J(r_{ij}) \mathbf{s}_i \cdot \mathbf{s}_j, \quad (9)$$

where \hat{H}_Z is Zeeman Hamiltonian, \hat{H}_{ex} is exchange magnetic Hamiltonian, μ_B is Bohr magneton, μ_0 is magnetic constant, g_i – Lande multiplier of the i -th spin, \mathbf{H}_{ext} is an external homogeneous magnetic field. This external field can be both constant and time-varying. The exchange Hamiltonian provides a natural connection between the spatial and spin degrees of freedom through the exchange integral $J(r_{ij})$, acting on the interatomic distance r_{ij} . The form of the magnetic Hamiltonian in (9) is variational. In the general case, the magnetic Hamiltonian may include additional terms responsible for various spin effects, the meaning and form of which will be given in a separate section below.

The equations of motion of atoms and their spins can be obtained by applying Poisson brackets to the generalized Hamiltonian of the form (1) and (2). This approach is described in detail in [34]. Taking into account relaxation processes from (4) and (5) leads the model of stochastic combined (lattice and magnetic) molecular dynamics to the following form:

$$\frac{d\mathbf{r}_i}{dt} = \{\mathbf{r}_i, \hat{H}\} = \frac{\mathbf{p}_i}{m_i}, \quad (10)$$

$$\frac{d\mathbf{p}_i}{dt} = \{\mathbf{p}_i, \hat{H}\} = \sum_{j \neq i}^N \left(-\frac{dU(\mathbf{r})}{dr_{ij}} + \frac{dJ(r_{ij})}{dr_{ij}} \mathbf{s}_i \cdot \mathbf{s}_j \right) \frac{\mathbf{r}_{ij}}{r_{ij}} - \frac{\kappa}{m_i} \mathbf{p}_i + \chi(t), \quad (11)$$

$$\frac{d\mathbf{s}_i}{dt} = \{\mathbf{s}_i, \hat{H}\} = \frac{1}{(1+\lambda^2)} \left((\boldsymbol{\omega}_i + \boldsymbol{\eta}(t)) \times \mathbf{s}_i + \lambda \mathbf{s}_i \times (\boldsymbol{\omega}_i \times \mathbf{s}_i) \right), \quad i=1,2,\dots,N, \quad (12)$$

where $\{, \}$ is Poisson bracket notation.

The change of atomic momenta in equation (11) is due not only to the derivative of the interatomic potential, but also to the dynamics of magnetic forces varying depending on the spin configurations of the particles. In this case, only exchange interactions are considered. Additions to the Hamiltonian and to the equations of motion for other types of magnetic interactions are given in [35, 36]. Thus, the spin-lattice dynamics of a system of magnetic particles is determined by the joint numerical solution of a set of differential equations (10) - (12) for each atom.

The ordinary and spin temperatures in the considered system provide averaged measures of the distribution of spatial and spin degrees of freedom of the atoms:

$$T_l = \frac{2}{3Nk_B} \sum_{i=1}^N \frac{\mathbf{p}_i^2}{2m_i}, \quad T_s = \frac{\hbar}{2k_B} \frac{\sum_{i=1}^N |\mathbf{s}_i \times \boldsymbol{\omega}_i|^2}{\sum_{i=1}^N \mathbf{s}_i \cdot \boldsymbol{\omega}_i}. \quad (13)$$

Various approaches for determining thermodynamic parameters are known from the literature [37-39]. The instantaneous lattice temperature in this work was determined as the average value of atom kinetic energy [40]. The expression proposed in [41] was used to calculate the instantaneous spin temperature.

Potential of the modified embedded atom method

When In this work, we used the potential of the Modified Embedded Atom Method (MEAM) as one of the most promising and actively developing [42, 43]. The potential

is based on the electron density functional theory and is multi-particle, so when describing it, the set of all radius-vectors of atoms $\mathbf{r} = \{\mathbf{r}_1, \mathbf{r}_2, \dots, \mathbf{r}_N\}$ is given in parentheses. The essence of the MEAM potential is defined by the group of the following equations:

$$U(\mathbf{r}) = \sum_i U_i(\mathbf{r}) = \sum_i \left(F_i(\bar{\rho}_i) + \frac{1}{2} \sum_{j, j \neq i} \phi_{ij}(r_{ij}) \right), \quad i = 1, 2, \dots, N, \quad (14)$$

$$F_i(\bar{\rho}_i) = \begin{cases} A_i E_i^0 \bar{\rho}_i \ln(\bar{\rho}_i), & \bar{\rho}_i \geq 0 \\ -A_i E_i^0 \bar{\rho}_i, & \bar{\rho}_i < 0 \end{cases}, \quad (15)$$

$$\bar{\rho}_i = \frac{\rho_i^{(0)}}{\rho_i^0} G(\Gamma_i), \quad G(\Gamma) = \begin{cases} \sqrt{1+\Gamma}, & \Gamma \geq -1 \\ -\sqrt{|1+\Gamma|}, & \Gamma < -1 \end{cases}, \quad \Gamma_i = \sum_{k=1}^3 t_i^{(k)} \left(\frac{\rho_i^{(k)}}{\rho_i^{(0)}} \right)^2, \quad (16)$$

where $U_i(\mathbf{r})$ is potential energy of individual atoms of the system, F_i is immersion function of the i -th atom, $\phi_{ij}(r_{ij})$ is pair potential between two atoms under consideration. The embedding function depends on the background electron density $\bar{\rho}_i$, so it takes into account the locations of all neighboring atoms of the system. When describing the embedding function, the following characteristics are used: A_i is empirical potential parameter and E_i^0 is sublimation energy, ρ_i^0 is background electron density of the initial structure, $t_i^{(k)}$ are weighting coefficients of the model.

The total background electron density $\bar{\rho}_i$ from (14)-(16) takes into account the contribution of different types of electron orbitals s, p, d, f . These orbitals correspond to one-electron densities $\rho_i^{(0)}, \rho_i^{(1)}, \rho_i^{(2)}, \rho_i^{(3)}$, which, in turn, are described by expressions:

$$\rho_i^{(0)} = \sum_{j, i \neq j} \rho_j^{A(0)}(r_{ij}) S_{ij}, \quad (17)$$

$$\left(\rho_i^{(1)} \right)^2 = \sum_{\alpha} \left[\sum_{j, i \neq j} \frac{r_{ij\alpha}}{r_{ij}} \rho_j^{A(1)}(r_{ij}) S_{ij} \right]^2, \quad (18)$$

$$\left(\rho_i^{(2)} \right)^2 = \sum_{\alpha, \beta} \left[\sum_{j, i \neq j} \frac{r_{ij\alpha} r_{ij\beta}}{r_{ij}^2} \rho_j^{A(2)}(r_{ij}) S_{ij} \right]^2 - \frac{1}{3} \left[\sum_{j, i \neq j} \rho_j^{A(2)}(r_{ij}) S_{ij} \right]^2, \quad (19)$$

$$(\rho_i^{(3)})^2 = \sum_{\alpha,\beta,\gamma} \left[\sum_{j,i \neq j} \frac{r_{ij\alpha} r_{ij\beta} r_{ij\gamma}}{r_{ij}^3} \rho_j^{A(3)}(r_{ij}) S_{ij} \right]^2 - \frac{3}{5} \sum_{\alpha} \left[\sum_{j,i \neq j} \frac{r_{ij\alpha}}{r_{ij}} \rho_j^{A(3)}(r_{ij}) S_{ij} \right]^2, \quad (20)$$

$$\rho_i^{A(k)}(r_{ij}) = \rho_{i0} \exp \left[-B_i^{(k)} \left(\frac{r_{ij}}{r_i^0} - 1 \right) \right], \quad k = 0, 1, 2, 3, \quad (21)$$

where $r_{ij\alpha}$ is component α ($\alpha, \beta, \gamma = x, y, z$) of the distance vector between two atoms, $\rho_i^{A(h)}$ is radial function, r_i^0 is distance to the nearest neighbor in the monocrystal, $B_i^{(k)}$ are empirical potential parameters for a certain type of atom, S_{ij} is potential screening function. The screening function provides a seamless smoothing of the potential over distance, which promotes a more physically reasonable behavior of energy in the system, without sudden jumps, and reduces the computational cost of running simulations.

The model weighting coefficients $t_i^{(k)}$ from (16) are determined using the following equation:

$$t_i^{(k)} = \frac{1}{\rho_i^{(0)}} \sum_{j,i \neq j} t_{0,j}^{(k)} \rho_j^{A(0)} S_{ij}, \quad (22)$$

where $t_{0,j}^{(k)}$ are potential parameters of the j -th atom, depending on its chemical type.

Thus, the potential of the modified embedded atom method has a rather large set of input parameters, which to some extent limits the manipulation of it. Nevertheless, at the moment a rather large database of MEAM parameters for various chemical elements has been accumulated, which certainly simplifies and actualizes its use.

Spin effects and calculation of the magnetic Hamiltonian

The methodology used includes modeling of atomic magnetic spins associated with spatial displacements of atoms (lattice). The dynamics of these magnetic spins can

be used to model a wide range of phenomena related to magnetoelasticity or to study the effect of defects on the magnetic properties of materials. Magnetic spins interact with each other and with the lattice through pairwise interactions. The general form of the Hamiltonian expression from (1) and (2) to describe the total energy of magnetic systems can be represented in the form of separate contributions:

$$\hat{H}_{\text{mag}} = \hat{H}_z + \hat{H}_{\text{ex}} + \hat{H}_{\text{an}} + \hat{H}_{\text{Neel}} + \hat{H}_{\text{dm}} + \hat{H}_{\text{me}} + \hat{H}_{\text{di}}, \quad (23)$$

where the first two terms in the right-hand side characterize the Zeeman and exchange interactions, the next two terms describe the magnetic anisotropy, followed by the terms responsible for the Dzyaloshinskii-Moria, magnetoelectric and dipole interactions [25, 44].

As it was noted earlier, in addition to \hat{H}_z and \hat{H}_{ex} in the general case, the expression for the description of the magnetic Hamiltonian can include additional terms responsible for various spin effects. The value of the exchange integral $J_{ij}(r_{ij})$ in equation (9) can be estimated using the Bethe-Slater curve:

$$J(r_{ij}) = 4\alpha \left(\frac{r_{ij}}{\delta} \right)^2 \left(1 - \gamma \left(\frac{r_{ij}}{\delta} \right)^2 \right) e^{-\left(\frac{r_{ij}}{\delta} \right)^2} \Theta(R_c - r_{ij}), \quad (24)$$

where α, δ, γ , – constant coefficients, $\Theta(R_c - r_{ij})$ – Heaviside function.

Depending on the crystal lattice of the material under study, different forms of magnetic anisotropy can occur. In [44, 45], approximations for modeling spin-orbit coupling were proposed. Thus, in particular, [45] used the functions proposed by Neel to model bulk magnetostriction and surface anisotropy in cobalt.

To describe the above phenomena, it is possible to use Neel's model of pairwise anisotropy between pairs of magnetic spins \hat{H}_{Neel} . To calculate the uniaxial magnetic anisotropy in the modeled systems, the Hamiltonian \hat{H}_{an} is used.

It is also well known that the combination of the exchange interaction and the spin-orbit interaction can lead to noncollinear spin states. The most common way to model such an effect is to relate the exchange interaction to another interaction, called the antisymmetric Dzyaloshinsky-Moria interaction \hat{H}_{dm} [46]. In particular, it is known that the Dzyaloshinsky-Moria interaction is a key mechanism for the stabilization of magnetic skyrmions.

In magnetoelectric materials and multiferroics, there is a relationship between their magnetic and electrical properties. Therefore, magnetoelectric effects should be taken into account when considering these types of materials \hat{H}_{me} . According to [25, 47], the mechanisms of magnetoelectric effects can be accounted for through the antisymmetric spin-spin effective interaction as a special case of the Dzyaloshynski vector.

In magnetic systems below the paramagnetic limit, the intensity of the dipole interaction \hat{H}_{di} is usually much smaller than that of the other magnetic interactions considered. For this reason, this effect can be safely omitted.

In the numerical experiments related to spin dynamics, a simplified form of the magnetic Hamiltonian was used in this work, i.e., only the Zeeman \hat{H}_z and exchange interactions \hat{H}_{ex} were considered. In some cases, taking into account additional contributions in the system allows one to calculate more accurately the properties of the materials under study, but it can be difficult. The problem is the need to find or determine a number of magnetic modeling parameters, which are often unknown, especially for multicomponent systems.

Integration algorithm and numerical realization

The set of equations (10) - (12) determines the dynamics of all magnetic particles of the system under consideration. Various discrete expansions and analogs are used to numerically solve these equations [48-50]. For simplicity of further description, it will be convenient to represent the system in the form of a generalized equation with one vector of variables $\mathbf{x}(t)$:

$$\frac{d\mathbf{X}(t)}{dt} = \hat{L}\mathbf{X}(t), \quad \mathbf{X}(t) = \begin{pmatrix} \mathbf{r}(t) \\ \mathbf{p}(t) \\ \mathbf{s}(t) \end{pmatrix}, \quad (25)$$

where \hat{L} is Liouville operator of the magnetic atom system. The general Liouville operator from (25) can also be represented as a sum of partial Liouville operators $\hat{L}_r, \hat{L}_p, \hat{L}_s$ acting each on its own group of variables:

$$\hat{L} = \sum_{i=1}^N \left(\frac{d\mathbf{r}_i}{dt} \cdot \frac{\partial}{\partial \mathbf{r}_i} + \frac{d\mathbf{p}_i}{dt} \cdot \frac{\partial}{\partial \mathbf{p}_i} + \frac{d\mathbf{s}_i}{dt} \cdot \frac{\partial}{\partial \mathbf{s}_i} \right) = \sum_{i=1}^N (\hat{L}_{r_i} + \hat{L}_{p_i} + \hat{L}_{s_i}) = \hat{L}_r + \hat{L}_p + \hat{L}_s. \quad (26)$$

Integrating the vector $\mathbf{x}(t)$ and obtaining the values of the unknowns at the next time step can be formally interpreted as applying the exponent of the Liouville operator to the vector $\mathbf{x}(t)$:

$$\mathbf{X}(t + \Delta t) = e^{(\hat{L}_r + \hat{L}_p + \hat{L}_s)\Delta t} \mathbf{X}(t), \quad (27)$$

where Δt is a time step.

The individual operators \hat{L} from (26) and (27) do not commute with each other. For this reason, the Suzuki-Trotter and Magnus decomposition [51] allows us to reduce the equation to the following one:

$$e^{(\hat{L}_r + \hat{L}_p + \hat{L}_s)\Delta t} = e^{\frac{\hat{L}_p \Delta t}{2}} e^{\frac{\hat{L}_s \Delta t}{2}} e^{\hat{L}_r \Delta t} e^{\frac{\hat{L}_s \Delta t}{2}} e^{\frac{\hat{L}_p \Delta t}{2}} + O(\Delta t^3). \quad (28)$$

In spite of the fact that by means of various permutations in (28) it is possible to obtain other varieties of decompositions, the expression presented here is

particularly effective. First, the time step required to integrate the spin system is usually an order of magnitude smaller than that usually used for the classical molecular dynamics of atomistic nonmagnetic systems [25]. Second, with this decomposition, the most time-consuming operations, such as force recalculation, only need to be performed once per time step, which ultimately improves the performance and efficiency of the algorithm. Third, in the absence of spins in the atoms of the system, the decomposition (28) takes the form of the well-known velocity algorithm of Werle [52].

The equations of motion for the spins are first-order differential equations that depend directly on the orientation of neighboring spins. The rotations of individual spins in three-dimensional space do not commute with each other, so the Liouville operator of the spin subsystem can be decomposed into the sum of individual operators \hat{L}_{s_i} , which leads to the following expression:

$$e^{\hat{L}_s \frac{\Delta t}{2}} = e^{\hat{L}_{s_1} \frac{\Delta t}{4}} \dots e^{\hat{L}_{s_N} \frac{\Delta t}{2}} \dots e^{\hat{L}_{s_1} \frac{\Delta t}{4}} + O(\Delta t^3) = \prod_{i=1}^N e^{\hat{L}_{s_i} \frac{\Delta t}{4}} \prod_{i=N}^1 e^{\hat{L}_{s_i} \frac{\Delta t}{4}} + O(\Delta t^3). \quad (29)$$

Each operator \hat{L}_{s_i} is a time integration operator of the spin vector with the number i .

The cumulative application of equations (27) through (29) at each time step yields a consistent solution of the equations of motion for the system of magnetic particles. The initial values of the velocity vectors and spin directions are set randomly from the considerations of correspondence to the ordinary and spin temperature at the initial time instant. The initial values of atomic coordinates are determined by the structure (liquid, solid, gaseous) of the nanomaterial under study and by the formulation of specific problems.

The model and numerical algorithms described in this work are implemented in the LAMMPS software package [53]. This software package was created by a team of authors from Sandia National Laboratories and is distributed under the GPL license,

i.e., it is available free of charge in the form of source codes. The additional package LAMMPS SPIN allows numerical studies of magnetic systems and calculation of spin dynamics of atoms [25, 54]. The scripts developed by the authors for the LAMMPS software package were used in the calculations and data analysis.

Study of ferromagnetic-superconductor structure and properties

The computational experiments performed in this work represent three separate series of calculations. In the first case, the processes of formation and structurization in a multilayer cobalt-iron-niobium nanocomposite were considered. The modeling was aimed at investigating the mechanisms of attachment and interaction of atoms in three-component layered systems. The second version of numerical experiments analyzed the mutual self-ordering of directions and reorientation of spins in crystalline iron in the presence and absence of a magnetic field. In this study, the mechanism of mutual response of atomic spins to each other and the manifestation of spontaneous magnetization, which is characteristic of ferromagnetics, and thus, including iron, was of interest. The third numerical experiment was focused on modeling the magnetic properties of a cobalt-iron bilayer film under conditions of a uniform external magnetic field. In this case, attention was focused on the study of the magnetic properties of the nanocomposite depending both on the mutual arrangement of atoms of different materials and on external magnetic factors.

The first computational experiment, the problem of studying the processes of ferromagnetic-superconductor structure formation, was solved for a three-layer system based on cobalt, iron, and niobium. The investigated composite is a layered structure with sequentially arranged films of nanoscale thickness of Co, Fe, Nb. Cobalt and iron

act as a substrate, the niobium layer acts as a superconducting material and is formed by deposition on a thin iron nanofilm. The relevance of the study of such systems is shown, for example, in [10]. The problem was solved by the method of classical molecular dynamics; the spin behavior of atoms was not considered in this problem.

At the initial moment of time, the system contained a 20 Å thick cobalt substrate (8000 atoms) and a 10 Å thick iron nanofilm (3200 atoms) located on it. The substrate and the film had a crystalline structure. The bottom layer of substrate atoms was partially fixed, its atoms could not move in the vertical direction. In the horizontal directions (ox and oy axes), periodic boundary conditions were applied in the system, and reflection boundary conditions were applied at the top and bottom. Before deposition of niobium (3000 atoms), the cobalt substrate and the iron nanofilm were at rest, and there were no external forces in the system. The initial and thermostat temperatures were set at 300 K. The thermostatization performed during the modeling process affected only the substrate, the iron nanofilm and the already deposited niobium atoms. The atoms in the gas phase were not subjected to temperature control. The general scheme of the computational experiment is illustrated in Figure 1.

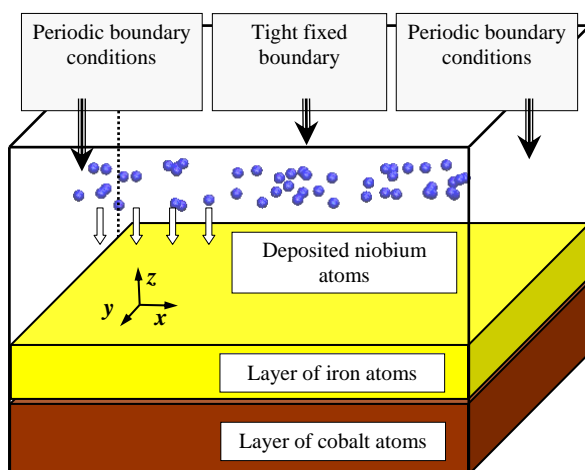


Figure 1: Schematic diagram of modeling the process of niobium nanofilm deposition on a bilayer nanocomposite of cobalt and iron

The result of modeling the deposition of niobium atoms on a layered cobalt and iron base is demonstrated in Figure 2. The uneven surface topography of the deposited niobium nanofilm is clearly visible. The nanofilm is formed rough, with height differences of several angstroms. Such an effect, according to the authors, can be explained by more intense interaction forces arising between niobium atoms compared to other types of atoms considered. Visual analysis of the system shows that the Co-Fe layers have not undergone significant rearrangement, the structure of these films predominantly remained crystalline. The structure of the deposited niobium nanofilm is difficult to judge visually, but there is no clear crystalline structure in it. Also, no deep penetration of niobium atoms inside Co-Fe was observed during the deposition process. This result is important because in some cases during sputtering, mixing of materials occurs and diffuse interfaces between nanofilms are formed. Diffuse interfaces can lead to disruption of the magnetization mechanisms of the composite, and thus subsequently degrade its basic functional properties.

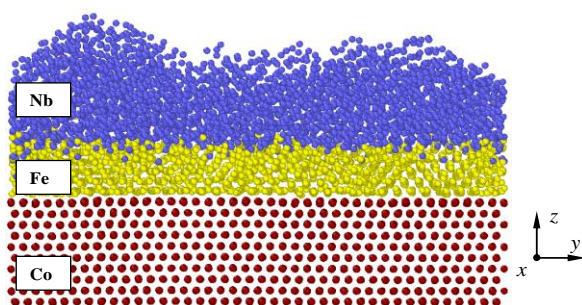


Figure 2: Appearance and structure of cobalt-iron-niobium nanocomposite obtained by modeling of niobium nanofilm deposition by the molecular dynamics method

Quantitative analysis of the formed nanocomposite composition was carried out layer by layer. For this purpose, horizontal thin layers of the system with a thickness of 2 Å were considered in the vertical direction and the quantitative fractions of the studied types of atoms in each layer were calculated. The calculation started from the bottom

layer and ended with the surface of the deposited niobium nanofilm. The fractions of deposited atoms in percentage by layers are shown in Figure 3.

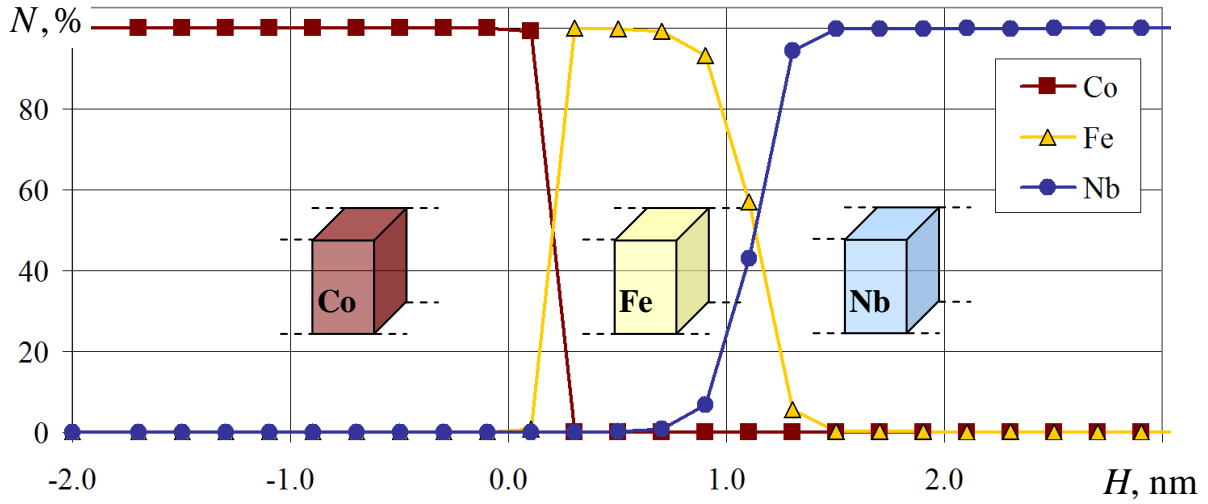


Figure 3: Height distribution of cobalt-iron-niobium nanocomposite composition, obtained after deposition of niobium nanofilm

The composition study presented in Figure 3 indicates a fairly clear separation of the different material nanofilms and confirms the results of the visual analysis of the atomic structure shown in Figure 2. Nevertheless, the formation of a more blurred contact zone is observed between the iron and niobium nanofilms compared to the contact between the cobalt and iron layers. The deposited niobium atoms have high kinetic energy, as a consequence of which there is a partial introduction of them into the surface layers of iron, on which sputtering is carried out.

To evaluate the structure of the atomistic material, we used the lattice centrosymmetry parameter calculated according to the following expression:

$$C_{\text{sim}} = \sum_{i=1}^{Z/2} |\mathbf{r}_i + \mathbf{r}_{i+Z/2}|^2, \quad (30)$$

where Z is the number of nearest neighbors for the atom under consideration; \mathbf{r}_i and $\mathbf{r}_{i+Z/2}$ are radius vectors of the analyzed and one of the nearby atoms. In expression

(30) the whole set of possible nearest neighbors of an atom is searched and the square of the distance between them is calculated in pairs. The obtained average value of the parameter characterizes the overall deviation of the nanomaterial structure from the ideal crystal structure.

In general, the behavior of the lattice centrosymmetry parameter depends on many factors, including temperature, since thermal fluctuations affect the coordinate deviations of atoms from their ideal positions. Nevertheless, for solid crystalline materials the average value of this parameter is small, while for amorphous materials it has a large positive value. For the investigated cobalt-iron-niobium nanocomposite, the distribution of the lattice centrosymmetry parameter for different axial projections is illustrated in Figure 4.

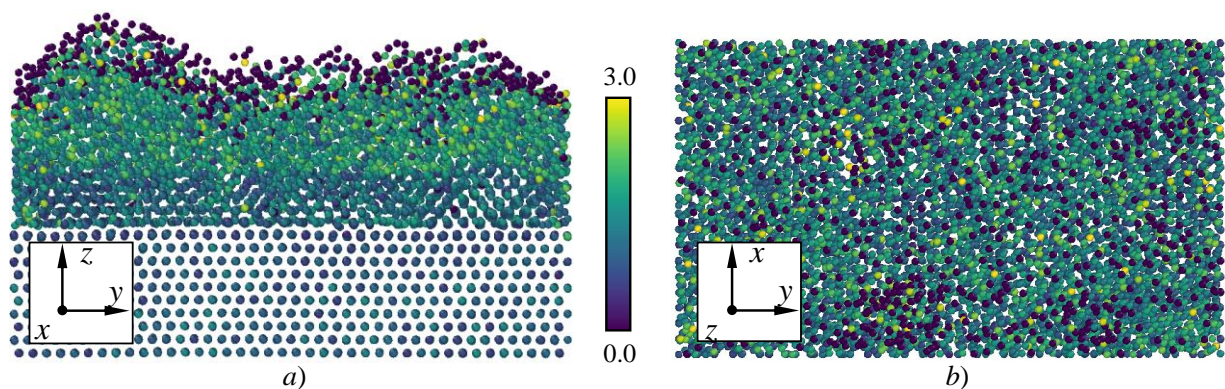


Figure 4: Distribution of the lattice centrosymmetry parameter of cobalt-iron-niobium composite atoms at the final moment of time after deposition for axial projections: a) yoz and b) yox

Analysis of the formed nanocomposite atomic structure in Figure 6 shows that the smallest value of the parameter C_{sim} has surface niobium atoms. This effect is explained by the incomplete set of nearest neighbors of these atoms, so the lattice centrosymmetry parameter cannot be used to study the surface structure of

nanomaterials. Cobalt and iron nanofilms have a small value of the lattice centrosymmetry parameter, which indicates that their structure is close to crystalline. The deposited niobium nanofilm is characterized by higher values of C_{sim} . Its non-ideal structure is clearly visible in Figure 6. The niobium layer undergoes significant rearrangement and subsequent slight compaction during deposition due to transformation processes occurring between atoms. Nevertheless, the final structure of niobium also exhibits lattice distortions. The dependence of the magnetic parameters of the sample on its atomic structure is shown, for example, in [57]. Defects in the structure and local arrangement of atoms arising during the deposition of nanofilms can cause deterioration of macroscopic magnetic parameters such as the magnetization modulus, magnetic permeability and its temperature coefficient, saturation induction, and others.

The averaged value of the lattice centrosymmetry parameter during the modeling process varied in the range from 0 to 15. Such a large value is primarily due to the influence of chaotically arranged deposited niobium atoms, which made a significant contribution to the calculated value. The niobium atoms appeared randomly in the deposition zone during the formation of the nanofilm, so their structure was far from the ideal crystalline structure. The value of the lattice centrosymmetry parameter of the deposited atoms subsequently decreased.

As part of the study of nanofilm deposition processes, computational experiments were performed in this work, in which the size of the systems was multiplied both in horizontal directions and with respect to the number of sputtered atoms. In all cases, similar results were obtained for the structure and composition of the formed nanocomposite. Thus, the influence of boundary effects on the properties of the formed three-layer sample was excluded. In the variant of increasing only the number

of deposited niobium atoms, the thickness of the final nanofilm increased, but its structure and uneven surface structure remained.

Modeling of nanomaterials deposition processes in this work was considered for physical vapor deposition (PVD) technology. This technology includes a rather large group of methods for obtaining materials (thermal sputtering, molecular beam epitaxy, magnetron sputtering, laser beam or vacuum arc evaporation, focused ion beam heating, and others) and is based on the transformation of the deposited material into the gas phase. The sputtering process by this technology, as a rule, takes place in a vacuum environment. At this stage of research, the method of atom deposition by directed flow, characteristic, for example, of molecular beam epitaxy technology, was considered in this work. In the future, it is planned to develop and expand the study of PVD technology to deposition methods using electromagnetic fields, including consideration of the method of magnetron sputtering.

As noted earlier, the second computational experiment analyzed the mutual self-ordering of directions and reorientation of spins in crystalline iron. The modeling considered a nanosystem consisting of 20 elementary iron cells in each horizontal direction and 3 crystalline cells in the vertical direction, resulting in about 3200 atoms. This stage of modeling is necessary to evaluate the correctness of the model and selected parameters of the computational experiment, as well as to investigate the influence of the external magnetic field on the considered system. The study of magnetic properties of the layered composite with sequentially arranged films of nanoscale thickness of Co, Fe, Nb was carried out at a temperature of 8 K. The choice of this value of the system temperature is due to the fact that at a temperature not exceeding 9.25 K, niobium transitions to the superconducting state. Therefore, and in the second computational experiment, the temperature was maintained at 8 K using a Langevin thermostat.

The second computational experiment included two parts: consideration of the crystalline iron nanosystem in the absence of an external magnetic field and in its presence. As a result of modeling, the spatial distribution of iron atoms spins during the whole time of the study was obtained. The direction of spin vectors at the initial moment of time was set randomly to minimize the probability of its influence on the final distribution of spin vectors. At the initial moment of time, the set of iron atoms and their spin vectors is shown in Figure 5.

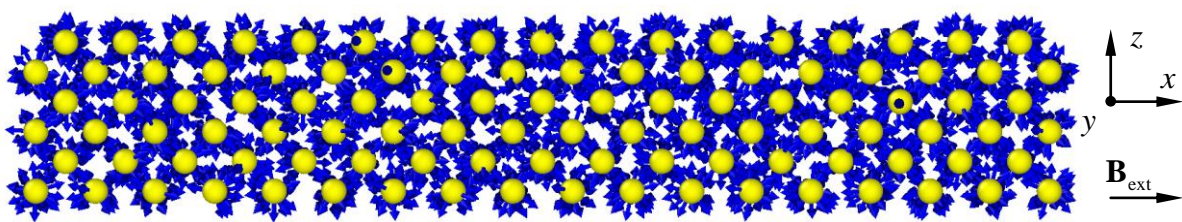


Figure 5: Distribution of iron atoms spin vectors at the initial moment of time in the computational experiment

In the process of modeling, as shown in Figure 6, the reorientation of atoms' spins is observed both in the absence of an external magnetic field and in its presence. Figures 6 a and 6 c show the formation of vortex currents (skyrmions), regions of spontaneous homogeneous magnetization, in which the magnetic moments of Fe atoms are co-directed, although no magnetic field was applied to the structure. Skyrmions are quantum excitations in a magnetic system that can be considered as collective excitations of magnetic moments [58]. They are quasiparticles that can move in a magnetic system, similar to electrons in a conductor. Skyrmions are found both in thin magnetic nanofilms [59] and in superconductors [60]. Materials in which skyrmions arise are promising for spintronics devices, including as an element of track memory [61] - the next generation magnetic memory.

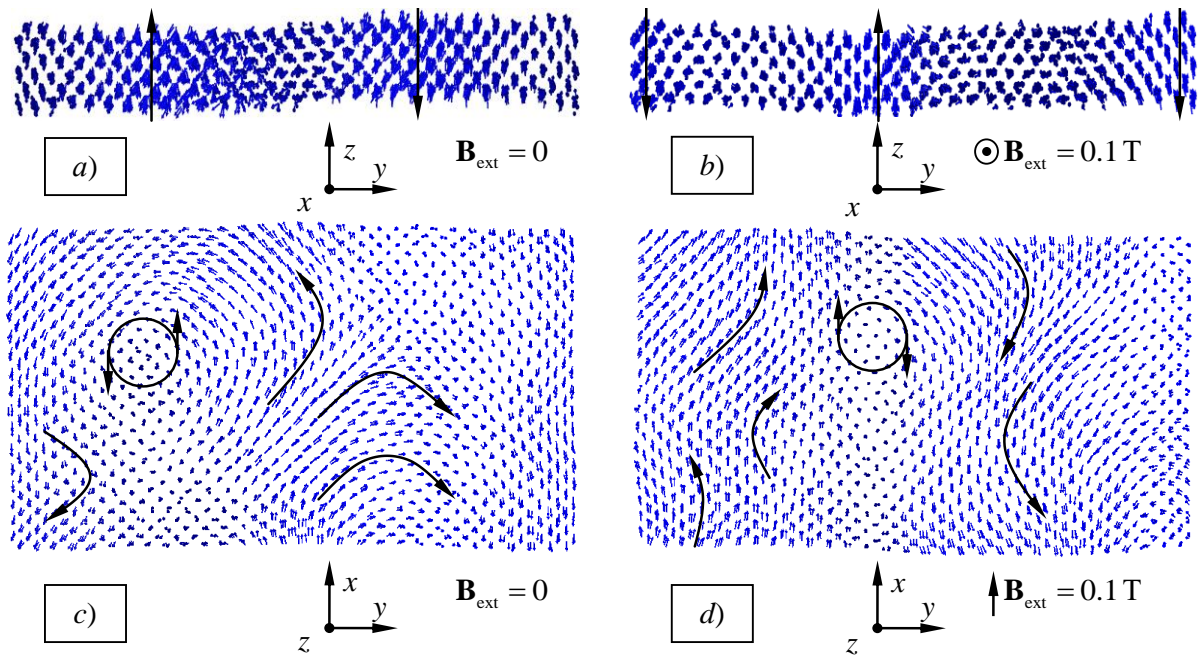


Figure 6: Direction of crystalline iron spin vectors for the time instant of 10 ps in the absence of an external magnetic field (a, c) and in its presence along the nanofilm surface (b, d)

The coordinated reorientation of atoms' spin vectors indicates the occurrence of spontaneous magnetization in iron. Such behavior of spins means that the material has ferromagnetic properties. The manifestation of ferromagnetic properties of iron is a known fact, which confirms the adequacy of the considered model, as well as the used parameters of potentials and magnetic interactions. Figures 6 b and 6 d show the distribution of magnetic moments in the system in an external magnetic field. The direction of the magnetic induction vector for this system coincided with the direction of the ox axis. The magnitude of the magnetic induction vector in the simulation was 0.1 T. Figure 6 shows that the application of an external magnetic field resulted in the displacement of the magnetic vortex regions. In the system with an applied external magnetic field, as well as in the system in the absence of a magnetic field, the formation of skyrmions is observed.

The overall magnetic behavior of the material can be analyzed using the system magnetization vector and magnetic energy. The variation of these parameters during the simulation is shown in Figure 7.

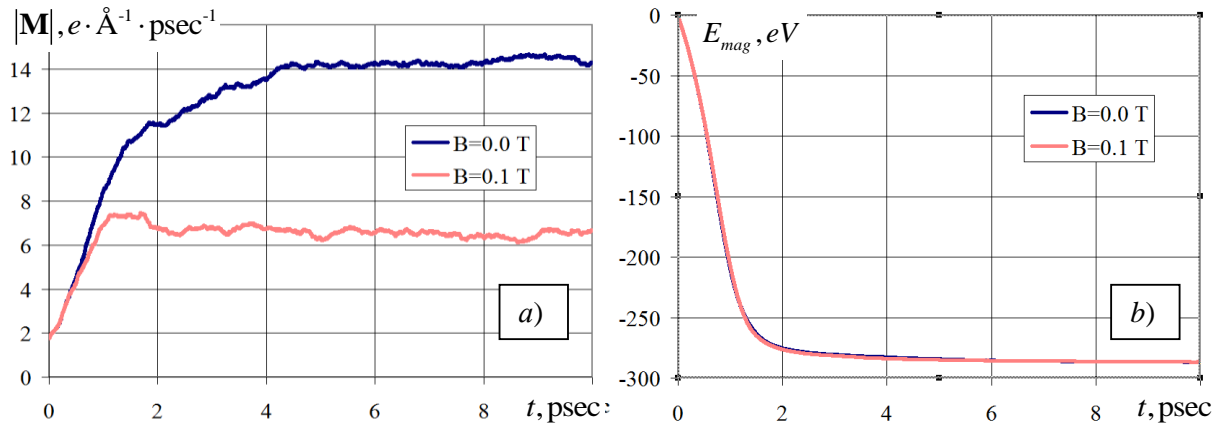


Figure 7: Variation of the magnetization norm a) and magnetic energy of the crystalline iron system b) during the simulation in the external magnetic field $B_{ext} = 0,1$ T and in its absence

Modeling has shown that under the influence of an external magnetic field, an induced magnetic moment appears in crystalline iron, the direction of which is opposite to the direction of the magnetic induction vector of the applied field. This phenomenon is caused by the Le Chatelier-Brown principle, according to which any equilibrium system under the condition of weak external influence tends to reduce it. This phenomenon explains the decrease in the magnetization norm of the system under the influence of an external magnetic field, which is clearly visible in Figure 7a. As can be seen from Figure 7 b, the total magnetic energy of the system during the computational experiment stabilizes around 280 eV both in the presence of an external magnetic field and without it. The abrupt change in the magnetic energy at the initial stage of the calculations is due to the nonequilibrium initial state of the

system under consideration, caused by the random distribution of spin vectors at the initial moment of time.

A more detailed behavior of the magnetization vector of the iron nanofilm is illustrated in Figure 8, where the dynamics of the individual components of this vector is presented. The behavior of the magnetization vector projections differed significantly between the case when the magnetic field was applied to the system and the variant with its absence.

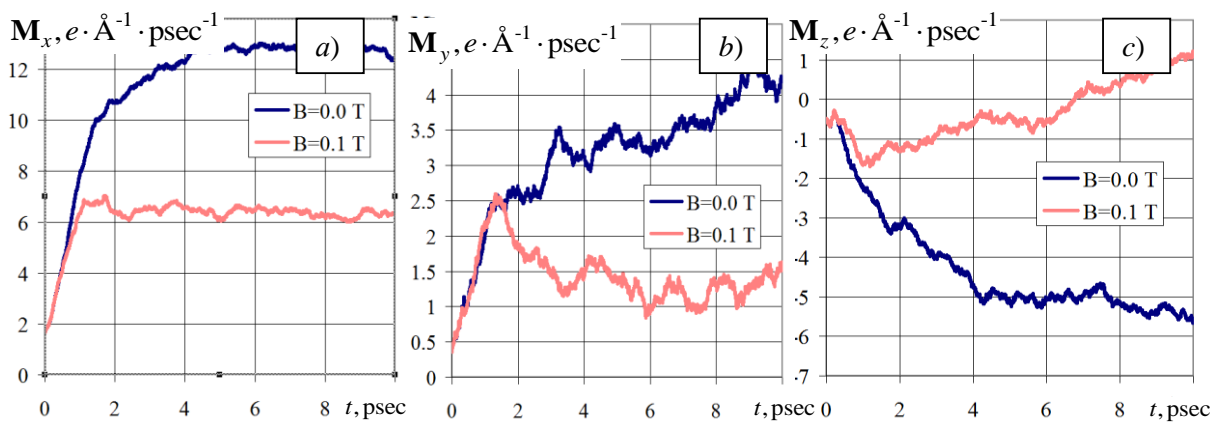


Figure 8: Components of the magnetization vector along the axes ox a), oy b) and oz c) in an external magnetic field and in its absence

The graphs in Figure 8 show that the magnetic moments of atoms are reoriented under the influence of an external magnetic field. Since the magnitude of the magnetization vector components along the oy and oz axes approaches zero (Figures 8 b and 8 c), we can conclude that the spin vectors of atoms are reversed along the oy axis. The revealed formation of skyrmions and their behavior under the influence of a magnetic field allows us to speak about the possibilities of promising use of crystalline iron nanofilms for memory devices functioning on the basis of the principle of controlled displacement of vortex magnetic regions under the influence of an external magnetic field.

Reproducibility of the obtained results of computational experiments is due to the fact that at any initial distributions of velocities and directions of atomic spins the system comes to a single equilibrium physical state. To confirm this fact, additional computational experiments with alternative distributions of initial velocities and spin vectors of atoms were carried out.

For the iron system under consideration, the magnetic moment was also calculated, and its value in units of the Bohr magneton was $2.2 \mu_B$. The obtained value corresponds well with the calculated data of first-principles modeling from [62, 63], where the magnetic moment was equal to the value of $2.17 \mu_B$. The experimental results described in [62] also give a close value of the momentum of $2.22 \mu_B$, which indicates satisfactory accuracy of the chosen mathematical model and adequate modeling parameters used.

The third computational experiment was focused on investigating the magnetic properties of a layered nanocomposite of cobalt (8000 atoms) and iron (3200 atoms) under conditions of a constant magnetic field. Such a system was considered in the first calculation as a basis for the deposition of the top niobium nanofilm. The magnetic induction vector $\mathbf{B}_{\text{ext}} = 0,1\text{T}$ was directed along the ox axis as shown in Figure 9. The materials had a crystalline structure and the MEAM potential was used for the interaction between atoms. Along the horizontal directions, the computational cell had periodic boundary conditions, and in the oz axis direction, reflection boundary conditions were in effect. The initial velocity and spin vectors of atoms were set randomly in accordance with the initial ordinary and spin temperatures $T = T_s = 8\text{ K}$, which coincided with the temperature values from the previous numerical experiment.

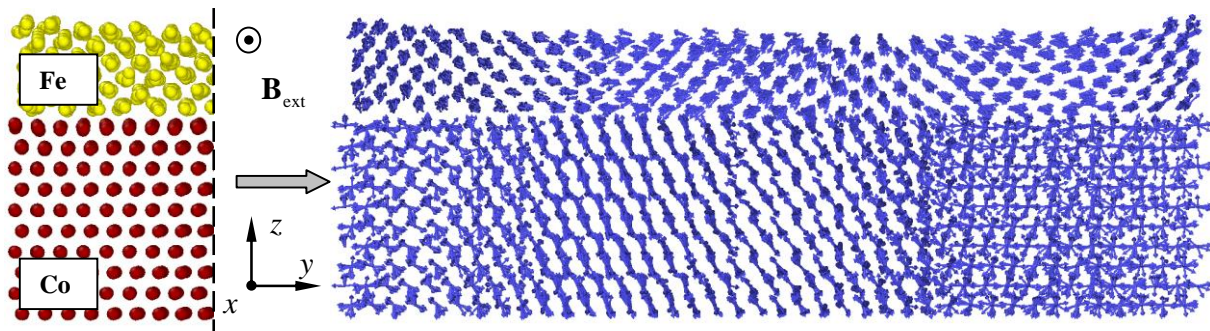


Figure 9: Distribution of atomic magnetic moments in thin film Co-Fe nanocomposite for a simulation time of 10 psec

During the simulation, the normal and spin temperatures were kept at the same level by using the Langevin dynamics. This value of temperatures was chosen specifically below the superconducting transition temperature of niobium (9.25 K). It is known that in superconductors, including niobium, the phenomenon of complete or partial displacement of the magnetic field from the material volume due to the Meissner effect occurs during the transition to the superconducting state [64]. For this reason, the niobium layer was not considered in the calculations performed.

The result of the spin dynamics of the two-component Co-Fe systems at a simulation time of 10 ps is shown in Figure 9. At the initial time moments, the magnetic moments of atoms in both the cobalt and iron nanofilms were differently oriented. Subsequently, a joint change in the orientation of the material atoms' spins was observed. The Fe layer was more typical to form vortex magnetic regions and skyrmions, which were previously obtained by modeling a single layer of crystalline iron. The magnetic behavior of the cobalt nanofilm differed from the pattern of mutual orientation of spins in iron. Sufficiently well-defined magnetic domain regions were obtained, which are well identified in Figure 10.

The magnetic domain zones shown in Figure 10 and selected by different geometrical shapes have different spatial orientation of spin vectors from each other.

At the same time, within the selected domains, a consistent uniform orientation of atomic spins is observed. The shape of the domains differs. At the junction of magnetic domains, the spin vectors of atoms are rotated. However, the overall magnetization of the system is low due to the absence of a distinct priority direction of magnetic moments. The zone structure of cobalt nanofilm magnetism is the reason for the increased polarization of spins of conduction electrons, which can be used in the creation of new film structures and magnetic nanoobjects in superdense recording and information storage devices.

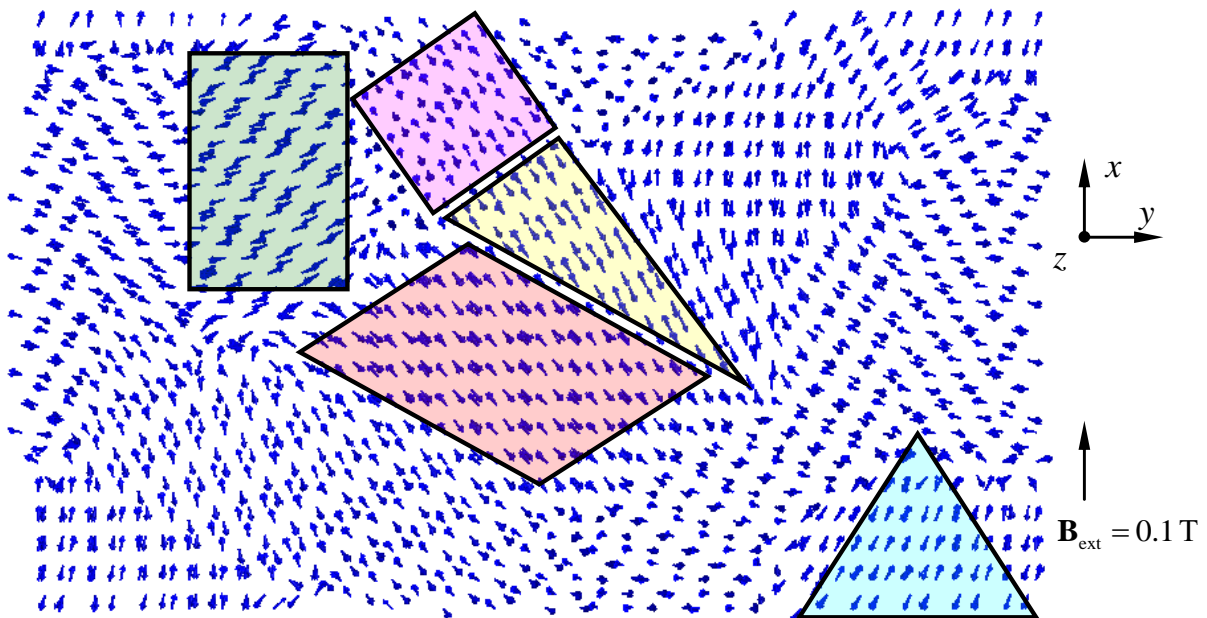


Figure 10: Formation of domain magnetic regions in a cobalt nanofilm at a simulation time of 10 psec

The average dynamics of atomic motion and changes in their spins can be estimated by calculating the temperatures of the system. The change of lattice T_l and spin T_s temperatures of the investigated cobalt-iron composite in the process of modeling is illustrated in Figure 11. Analysis of the temperature graph shows that significant changes and jumps of these parameters are observed at the initial moments of time.

Such an effect is explained by stochastic initial distributions of velocities and magnetic moments of atoms. In the future, the velocities and directions of spins, which were unstable in the initial state, are rearranged, and fluctuations of the values become moderate. The temperature dynamics reaches stationary regimes corresponding to thermostat values of 8 K. Insignificant fluctuations of temperatures near the target value indicate that the composite is in an energy stable state, and the lattice and spin thermostats function adequately in the system.

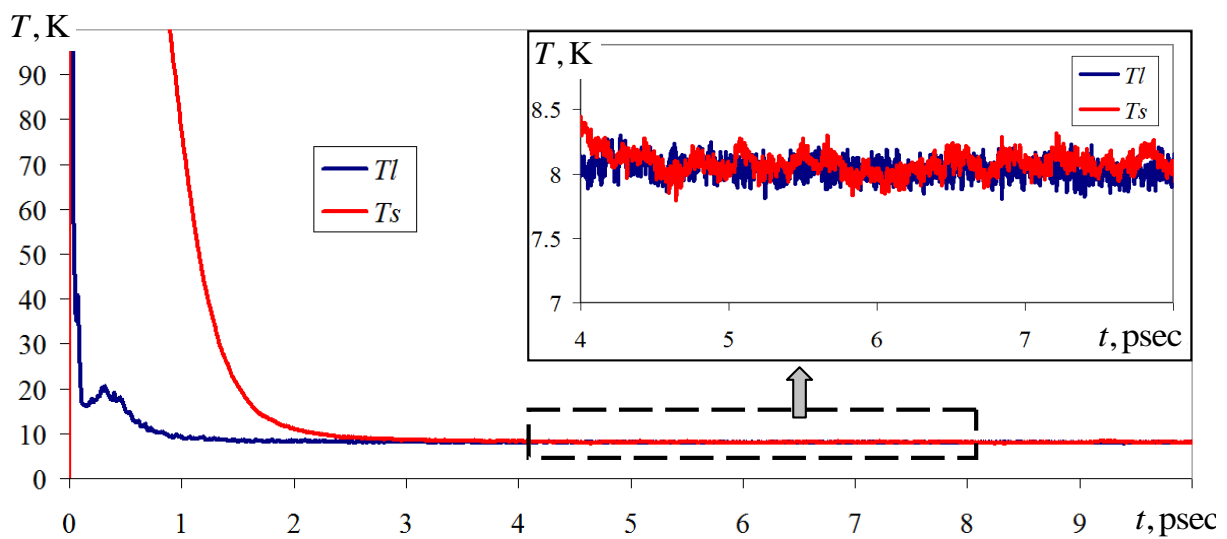


Figure 11: Graphs of spin and lattice temperature dependences from time for Co-Fe nanocomposite

For the layered cobalt-iron nanocomposite in this work, the change in the magnetization norm was calculated, which is shown in Figure 12. The magnetization rate was determined both for the composite as a whole (Co+Fe (h=1 nm) label) and separately for cobalt (Co label) and iron (Fe (h=1 nm) label). Additionally, the magnetic behavior of the same system but with a 2-fold increased thickness of the iron nanofilm (tag Fe (h=2 nm)) was investigated. The magnetic moments of the domain structure arising in cobalt are multidirectional, which causes the

magnetization norm value of this nanofilm to be close to zero. As can be seen from Figure 12, the domains are built rather quickly (within the first picosecond of modeling), and further the magnetization norm of cobalt changes insignificantly.

The dynamics of the magnetization norm of iron nanofilms has a more variable character. This is due to the fact that the vortex orientation of the atomic spins requires a longer time to occur. In addition, already after the formation of skyrmions in iron, some displacement can occur, which also affects the change of the magnetization norm. The skyrmions in iron have a well-defined magnetic moment, which leads to larger values of the magnetization rate of iron, compared to the cobalt nanofilm. This effect is clearly visible in Figure 12. In the variant of the computational experiment with increased Fe thickness, vortex structures appear not only in the plane of the nanofilm, but also unfolded in the volume, which causes reorientation of the magnetic moments of atoms and, as a consequence, an increase in the magnetization norm of the material.

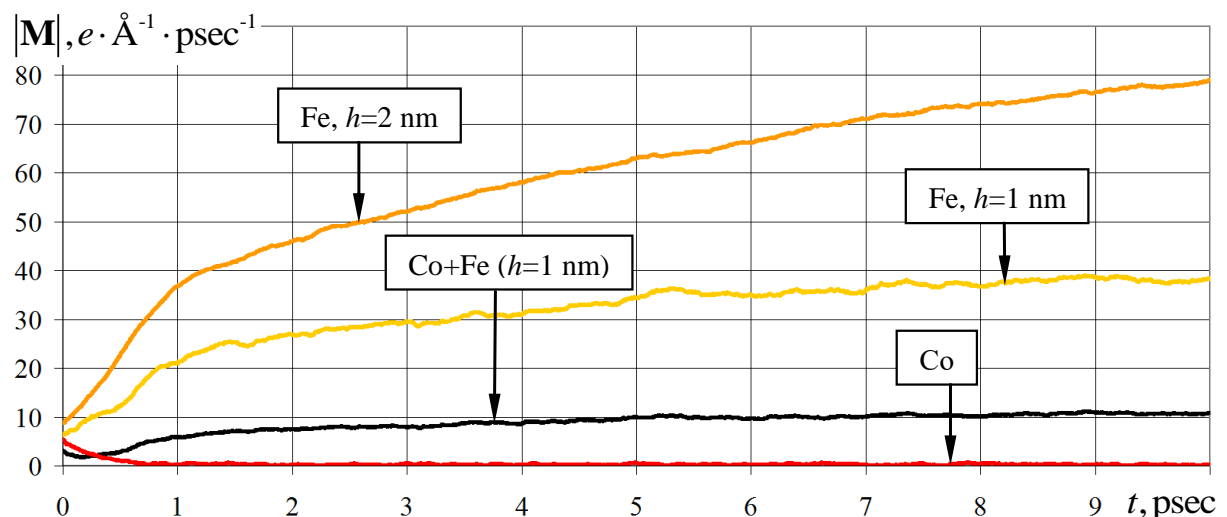


Figure 12: Variation of the magnetization norm in layers of cobalt, iron of different thicknesses and nanocomposite as a whole

The use of skyrmions, obtained from the modeling in the second and third problems, and Josephson contacts [65] is a very effective direction in the creation of fast and energy-efficient memory devices, as well as in the development of superconducting qubits and quantum circuits focused on new generations of quantum CPUs [66]. Such nanostructures can also be used as tunable kinetic inductors, which are designed to implement and control artificial neural networks with magnetic data representation [67]. However, the creation of nanoscale thin-film multilayer materials and precise control of their magnetic states requires a thorough elaboration of their fabrication technologies, functioning processes, as well as expanding the understanding of the fundamental properties of nanoobjects.

Conclusion

The literature analysis on magnetoresistive memory shows that these types of data storage devices are actively developing and improving. In this paper, a comparative characterization of different types of magnetoresistive random access memory was carried out. In all types of considered MRAMs it is possible to use the ferromagnetic-superconductor structure as a spin valve or magnetic tunnel junction. Active use of magnetoresistive memory requires a detailed analysis of magnetization processes, spin reorientation mechanisms, typicalized composition and structure of MRAM cells, in which their disadvantages can be reduced or minimized and the performance of memory devices can be optimized.

The paper considers a combined model of spin dynamics and classical molecular dynamics, which allows to simultaneously describe the structure of a material and its magnetic properties. The modeling method is based on the joint solution of the equations of atomic motion and changes in their spins, includes algorithms for

adjusting spin and lattice temperatures, and is implemented in the freely distributed software package LAMMPS. To describe the interactions in the model and the software package, a potential from a rather large set of already realized potentials (Buckingham, Lennard-Jones, Morse, Yukawa, EAM, MEAM, AI-REBO, Stillinger-Weber, Tersoff, CHARMM and others) can be used. In this paper, MEAM was chosen as a potential as it is one of the most accurate, well-established and actively used for such tasks. In spite of the fact that for numerical studies a simplified form of the magnetic Hamiltonian, which takes into account only Zeeman and exchange interactions, was considered, in the general case magnetic anisotropy, Dzyaloshinskii-Moria interactions, magnetoelectric and dipole interactions can also be described using the proposed spin dynamics. The undoubted advantage of the model is the possibility to study large systems, which is problematic to do using classical methods of quantum mechanics. The weaknesses of the model include the need to find or determine a number of magnetic modeling parameters that are often unknown, especially for multicomponent systems.

Numerical study of niobium deposition processes on a bilayer composite of cobalt and iron has shown that cobalt and iron nanofilms have small values of the lattice centrosymmetry parameter. This fact indicates that their structure is close to the crystalline structure. The deposited niobium nanofilm is characterized by higher values of the lattice centrosymmetry parameter, non-ideal structure and uneven surface. A layer-by-layer study of the composition shows a fairly clear separation of nanofilms of different materials, but between the layers of iron and niobium the formation of a more blurred contact zone is observed. The deposited niobium atoms have high kinetic energy, which results in their partial introduction into the surface of the iron, on which the sputtering is carried out.

In the computational experiment investigating the magnetic behavior of iron crystalline nanofilm atoms under conditions of external field and its absence, it was obtained that in both considered variants the reorientation of spins was observed, the formation of spontaneous homogeneous magnetization regions and vortex currents occurred. The coordinated reorientation of spin vectors indicates the occurrence of spontaneous magnetization in iron and the manifestation of ferromagnetic properties. The presence of an external magnetic field led to the displacement of magnetic vortex regions, the reversal of atomic spins, and a decrease in the norm of the total magnetization of the nanomaterial. This phenomenon is caused by the Le Chatelier-Brown principle, according to which any equilibrium system under the condition of a weak external influence tends to reduce this influence.

As a result of modeling the magnetic properties of a layered nanocomposite of cobalt and iron under conditions of a constant magnetic field, the formation of skyrmions in the iron nanofilm and domain regions in cobalt was observed. The shape of the domains differed. The magnetic moments of the domain structure appearing in cobalt were multidirectional, which caused the magnetization norm value of this nanofilm to be close to zero. The iron layer in the nanocomposite had larger values of the magnetization norm compared to cobalt, since the formed skyrmions had a distinct magnetic moment. In a variant of the computational experiment with increased iron thickness, vortex structures were obtained not only in the plane of the nanofilm, but also deployed in the volume.

Materials in which skyrmions arise are promising for spintronics devices, including as an element of racetrack memory. The use of skyrmions and Josephson contacts is also a very effective direction in the development of superconducting qubits and quantum circuits for quantum CPUs, kinetic inductors for artificial neural networks with magnetic data representation.

Funding

The work was carried out within the framework of the state assignment № FUUE-2022-0008 "Modeling of processes of formation and functioning of superconducting nanostructures" and with the financial support of the Russian Science Foundation (project No. 22-79-10018 "Controlled kinetic inductance based on superconducting hybrid structures with magnetic materials" (theory development, results evaluation), and project No. 020201 of the Moldova State Program "Nanostructures and advanced materials for implementation in spintronics, thermoelectricity and optoelectronics" (samples preparation and investigation of Nb/Co interfaces).

References

1. Fersht, V. M.; Latkin, A. P.; Ivanova, V. N. *Territoriya novyh vozmozhnostej. Vestnik Vladivostokskogo gosudarstvennogo universiteta ekonomiki i servisa [Territory of New Opportunities. Bulletin of Vladivostok State University of Economics and Service]*, **2020**, 12, 121-130.
2. Korobchenko, E.V. *Ekonomicheskaya bezopasnost' i kachestvo [Economic security and quality]*, **2018**, 3, 49-51.
3. Farrelly, T. *Quantum*, **2020**, 4, 368.
4. Binasch, G.; Grünberg, P.; Saurenbach, F.; Zinn, W. *Phys. Rev. B*, **1989**, 39, 4828-4830.
5. Chappert, C.; Fert, A.; Van Dau, F.N. *Nature materials*, **2007**, 6, 813-823.
6. Cubukcu, M.; Boulle, O.; Mikuszeit, N.; Hamelin, C.; Brächer, T.; Lamard, N. et al. *IEEE Transactions on Magnetism*, **2018**, 54, 1-4.

7. Khvalkovskiy, A.V.; Apalkov, D.; Watts, S.; Chepulskii, R.; Beach, R.S.; Ong, A. et al. *Journal of Physics D: Applied Physics*, **2013**, 46, No. 074001.
8. Endoh, T.; Honjo, H.; Nishioka, K.; Ikeda, S. *2020 IEEE Symposium on VLSI Technology. IEEE*, **2020**, 1-2.
9. Mishchenko, E.G. *Phys. Rev. B*, **2003**, 68, No. 100409 (R).
10. Vodopyanov, B.P.; Tagirov, L.R.; Durusoy, H.Z.; Berezhnov, A.V. *Physica C*, **2001**, 366, 31- 42.
11. Xiong, D.; Jiang, Y.; Shi, K.; Du, A.; Yao, Y.; Guo, Z et al. *Fundamental Research*, **2022**, 2, 522-534.
12. Vakhrushev, A.V.; Fedotov, A.Yu.; Severyukhin, A.V.; Suvorov, S.V. *Himicheskaja fizika i mezoskopija [Chemical Physics and Mezoscopy]*, **2014**, 16, 364-380.
13. Vakhrushev, A.V.; Fedotov, A.Yu.; Savva, Ju.B.; Sidorenko, A.S. *Himicheskaja fizika i mezoskopija [Chemical Physics and Mezoscopy]*, **2019**, 21, 362-374.
14. Vakhrushev, A.V.; Fedotov, A.Yu.; Boian, V.; Morari, R.; Sidorenko, A.S. *Beilstein Journal Nanotechnology*, **2020**, 11, 1776-1788.
15. Vakhrushev, A.V.; Fedotov, A.Yu.; Savva, Ju.B.; Sidorenko, A.S. *Vestnik Permskogo nacional'nogo issledovatel'skogo politehnicheskogo universiteta. Mehanika [Bulletin of the Perm National Research Polytechnic University. Mechanics]*, **2020**, 2, 16-27.
16. Vakhrushev, A.V.; Severyukhin, A.V.; Fedotov, A.Yu.; Valeev, R.G. *Vychislitel'naja mehanika sploshnyh sred [Computational Continuum Mechanics]*, **2016**, 9, 59-72.
17. Vakhrushev, A.V.; Fedotov, A.Yu. *Vychislitel'naja mehanika sploshnyh sred [Computational Continuum Mechanics]*, **2008**, 1, 34-45.

18. Prejbeanu, I.L.; Kerekes, M.; Sousa, R.C.; Sibuet, H.; Redon, O.; Dieny, B.; Nozières, J.P. *Journal of Physics: Condensed Matter*, **2007**, *19*, No. 165218.
19. Zhu, D. Q.; Guo, Z. X.; Du, A.; Xiong, D. R.; Xiao, R.; Cai, W. L. et al. *2021 IEEE International Electron Devices Meeting (IEDM)*. *IEEE*, **2021**, 17.5.1-17.5.4.
20. Nahas, J.; Andre, T.; Subramanian, C.; Garni, B.; Lin, H.; Omair, A.; Martino, W. A. *2004 IEEE International Solid-State Circuits Conference (IEEE Cat. No. 04CH37519)*. *IEEE*, **2004**, 44-512.
21. Prenat, G.; Jabeur, K.; Vanhauwaert, P.; Di Pendina, G.; Oboril, F.; Bishnoi, R. et al. *IEEE Transactions on Multi-Scale Computing Systems*, **2015**, *2*, 49-60.
22. Apalkov, D.; Khvalkovskiy, A.; Watts, S.; Nikitin, V.; Tang, X.; Lottis, D. et al. *ACM Journal on Emerging Technologies in Computing Systems (JETC)*, **2013**, *9*, 1-35.
23. Omelyan, I. P.; Mryglod, I. M.; Folk, R. *Physical Review Letters*, **2001**, *86*, 898-901.
24. Perera, D.; Landau, D. P.; Nicholson, D. M.; Stocks, G. M.; Eisenbach, M.; Yin, J.; Brown G. *Journal of Physics: Conference Series*, **2014**, *487*, 012007.1-9.
25. Tranchida, J.; Plimpton, S. J.; Thibaudeau, P.; Thompson, A. P. *Journal of Computational Physics*, **2018**, *372*, 406-425.
26. Antropov, V. P.; Katsnelson, M. I.; Van Schilfgaarde, M.; Harmon, B. N. *Physical Review Letters*, **1995**, *75*, 729–732.
27. Antropov, V. P.; Katsnelson, M. I.; Van Schilfgaarde, M.; Harmon B. N., Kusnezov D. *Physical Review B*, **1996**, *54*, 1019.
28. Bussi, G.; Parrinello, M. *Physical Review E*, **2007**, *75*, 056707.1-7.
29. Paquet, E.; Viktor, H. L. *BioMed Research International*, **2015**, *2015*, 183918.1-18.
30. Gilbert, T.L. *IEEE transactions on magnetics*, **2004**, *40*, 3443-3449.

31. Néel, L. *Comptes Rendus Hebdomadaires Des Seances De L Academie Des Sciences*, **1949**, 228, 664-666.
32. Brown, Jr. W. F. *Physical Review*, **1963**, 130, 1677-1686.
33. García-Palacios, J. L.; Lázaro, F. J. *Physical Review B*, **1998**, 58, 14937-14958.
34. Yang, K. H., Hirschfelder, J. O. *Physical Review A*, **1980**, 22, 1814-1816.
35. Perera, D.; Eisenbach, M.; Nicholson, D. M.; Stocks, G. M.; Landau, D. P. *Physical Review B*, **2016**, 93, 060402.1-5.
36. Beaujouan, D.; Thibaudeau, P.; Barreteau, C. *Physical Review B*, **2012**, 86, 174409.1-11.
37. Jepps, O. G.; Ayton, G.; Evans, D. J. *Physical Review E*, **2000**, 62, 4757-4763.
38. Rugh, H. H. *Journal of Physics A: Mathematical and General*, **1998**, 31, 7761.1-7.
39. Ma, P. W.; Dudarev, S. L.; Semenov, A. A.; Woo, C. H. *Physical Review E*, **2010**, 82, 031111.1-6.
40. Rugh, H. H. *Physical Review Letters*, **1997**, 78, 772-774.
41. Nurdin, W. B.; Schotte, K. D. *Physical Review E*, **2000**, 61, 3579-3582.
42. Lee, B-J.; Baskes, M. I.; Kim, H.; Cho, Y. K. *Physical Review B*, **2001**, 64, 184102.1-11.
43. Baskes, M. I. *Physical Review B*, **1992**, 46, 2727-2742.
44. Perera, D.; Eisenbach, M.; Nicholson, D. M.; Stocks, G. M.; Landau, D. P. *Physical Review B*, **2016**, 93, 060402.1-5.
45. Beaujouan, D.; Thibaudeau, P.; Barreteau, C. *Physical Review B*, **2012**, 86, 174409.1-11.
46. Rohart, S.; Thiaville, A. *Physical Review B*, **2013**, 88, 184422.1-8.
47. Katsura, H.; Nagaosa, N.; Balatsky, A. V. *Physical Review Letters*, **2005**, 95, 057205.1-4.

48. Tsai, S. H.; Krech, M.; Landau, D. P. *Brazilian Journal of Physics*, **2004**, *34*, 384-391.
49. Tsai, S. H.; Lee, H. K.; Landau, D. P. *American Journal of Physics*, **2005**, *73*, 615-624.
50. Garanin, D. A. *Physical Review E*, **2021**, *104*, 055306.1-9.
51. Blanes, S.; Casas, F.; Oteo, J. A.; Ros, J. *Physics Reports*, **2009**, *470*, 151-238.
52. Swope, W. C.; Andersen, H. C.; Berens, P. H.; Wilson, K. R. *The Journal of Chemical Physics*, **1982**, *76*, 637-649.
53. Plimpton, S. *Journal of Computational Physics*, **1995**, *117*, 1-19.
54. Beaujouan, D.; Thibaudeau, P.; Barreteau, C. *Physical Review B*, **2012**, *86*, 174409.1-11.
55. Vakhrushev, A. V.; Fedotov, A. Yu.; Severyukhina, O. Yu.; Sidorenko, A. S. *Beilstein Journal of Nanotechnology*, **2023**, *14*, 23-33.
56. Kang, W.; Huang, Y.; Zhang, X.; Zhou, Y.; Zhao, W. *Proceedings of the IEEE*, **2016**, *104*, 2040-2061.
57. Kiselev, N. S.; Bogdanov, A.N.; Schäfer, R.; Rößler, U. K. *Journal of Physics D: Applied Physics*, **2011**, *44*, No. 392001.
58. Kubetzka, A.; Bürger, J. M.; Wiesendanger, R.; von Bergmann, K. *Physical Review Materials*, **2020**, *4*, 081401.
59. Tomasello, R.; Martinez, E.; Zivieri, R.; Torres, L.; Carpentieri, M.; Finocchio, G. *Scientific Reports*, **2014**, *4*, 1-7.
60. Ursaeva, A. V.; Ruzanova, G. E.; Mirzoev, A. A. *Vestnik Yuzhno-Ural'skogo Gosudarstvennogo Universiteta. Seriya Matematika. Mekhanika. Phisika [Bulletin of the South Ural State University. Series: Mathematics. Mechanics. Physics]*, **2010**, *2*, 97-101.
61. Herper, H. C., Hoffmann, E.; Entel, P. *Physical Review B*, **1999**, *60*, 3839-3848.

62. Thompson, D. J.; Minhaj, M. S. M.; Wenger, L. E.; Chen, J. T. *Physical Review Letters*, **1995**, *75*, 529-532.
63. Soloviev, I. I.; Ruzhickiy, V. I.; Bakurskiy, S. V.; Klenov, N. V.; Kupriyanov, M. Y.; Golubov, A. A.; Skryabina, O. V.; Stolyarov, V. S. *Physical Review Applied*, **2021**, *16*, 014052.1-11.
64. Vozhakov, V. A.; Bastrakova, M. V.; Klenov, N. V.; Soloviev, I. I.; Pogosov, W. V.; Babukhin, D. V.; Zhukov, A. A.; Satanin, A. M. *Uspekhi fizicheskikh nauk [Advances in the Physical Sciences]*, **2022**, *65*, 421-439.
65. Bakurskiy, S. V.; Kupriyanov, M. Y.; Klenov, N. V.; Soloviev, I. I.; Schegolev, A. E.; Morari, R.; Khaydukov, Y. N.; Sidorenko, A. S. *Beilstein Journal of Nanotechnology*, **2020**, *11*, 1336-1345.